

Monte Carlo calculations of dose and linear energy transfer in double scattering proton therapy for prostate cancer

Title character count excluding spaces: 130 / 145 max

Rasmus Klitgaard^{1,2}, Lars Fredrik Fjæra^{3,4}, Camilla Hanquist Stokkevåg⁴, Perry Johnson⁵, Mark Artz⁵, Nancy Price Mendenhall⁵, Curtis Bryant⁵, Ludvig Paul Muren^{1,2}

1: Department of Clinical Medicine, Aarhus University, Aarhus, Denmark; 2: Danish Centre For Particle Therapy, Aarhus University Hospital, Aarhus, Denmark; 3: Department of Medical Physics, Oslo University Hospital, Oslo, Norway; 4: Department of Physics and Technology, University of Bergen, Bergen, Norway; 5: Department of Radiation Oncology, College of Medicine, University of Florida Health, Jacksonville, Florida, USA

11/12/23

Abstract

470 words / 500 words max

Background

The linear energy transfer transfer (LET) in proton therapy (PT) has in pre-clinical studies been linked to the relative biological effectiveness (RBE) of protons. The most common proton therapy delivery method in prostate cancer patients up until now has been double scattered PT and LET can be calculated using Monte Carlo (MC) simulations. However, as most studies in LET and RBE in double scattered PT have been focused on the head and neck region, the MC implementations are not all capable of calculations with the longer field ranges used in the pelvic region.

Purpose

The intial aim of this study was to implement MC code allowing for LET calculations in double scattered PT of prostate cancer. Additionally, we sought to explore LET profiles and the organ-to-organ LET differences as a function of field configuration, by performing MC calculations for a large prostate cancer cohort treated with double scattered PT.

Methods

We implemented the components of a passive scattered clinical treatment nozzle used for delivery of extended field ranges, with two associated modulation wheels, into an existing FLUKA MC framework. The code was validated to spread out Bragg peak (SOBP) measurements conducted using the treatment nozzle with 11 different range and modulation width configurations. After validation, we calculated LET for 582 prostate cancer patients treated with two-field double scattered PT. All patients had symmetric field configurations with respect to the sagittal plane, with one pair of either posterior oblique, lateral opposing or anterior oblique fields. We compared dose-LET volume parameters and the mean LET ratio between the bladder and rectum for the three groups.

Results

We achieved range differences below 1 mm for all calibration cases, and modulation width differences below 2 mm for 9 of 11 cases. For the patient simulations this resulted in 3mm/3% and 2mm/2% gamma pass ratings with a mean of 95.4 % and 89 % in the body and >98% and >93% for the PTV, bladder and rectum, respectively. We observed increasing mean LET values in both the 10 and 70 Gy isodoses of the bladder, and conversely, decreasing values in the rectum, when moving from anterior to posterior field configurations, with the largest differences being at the 10 Gy dose levels. We found a clear distinction in the mean LET ratios between bladder and rectum for anterior oblique, lateral opposing and posterior oblique field configurations, with ratios of 1.13 in the 9.6 Gy isodose for the anterior oblique group and 0.91 in the 5.2 Gy isodose for the posterior oblique group.

Conclusions

We successfully implemented MC code allowing for accurate simulations of dose and LET in double scattered PT of prostate cancer. We found a clear trend in the LET distributions across the rectum and bladder as the field configuration changed, and a systematic difference in the mean LET ratio between the bladder and rectum for different field configurations.

1. Introduction

Proton therapy (PT) is potentially a more conformal treatment modality for cancer than photon-based radiotherapy (RT), due to the characteristic charged particle interactions with matter. PT is therefore currently being explored for a number of tumour sites in several anatomical regions, including the pelvis in general and prostate in particular¹⁻⁶. Although most new PT installations are applying pencil beam scanning beam delivery, the majority of prostate cancer patients having received PT have been treated with double scattered PT. The normal tissue sparing potential of both modalities of PT depends not only on the improved treatment conformity, but also on a thorough knowledge about the relative biological effectiveness (RBE) of protons compared to photons. PT has a higher effectiveness compared to photon-based RT, with a current recommended value for the RBE of 1.1⁷. However, *in vitro* cell studies have shown that the RBE varies with both dose, fractionation, tissue type and linear energy transfer (LET)⁸. The dependencies of RBE to these factors, including LET, is currently receiving considerable attention⁹⁻¹³.

LET is a parameter that expresses the physical energy deposition per unit length. As a function of track-length along the proton beam, LET increases along with dose in the Bragg-Peak, and achieves its maximum at the distal end of the Bragg Peak. The three-dimensional LET distribution is determined by the treatment plan, including the beam configuration and each beam's characteristics, using Monte Carlo (MC) simulations, considered as the gold standard calculation method. MC simulations of double scattering PT delivery systems are more time- and resource-intensive compared to pencil beam scanning implementations since phase-space approaches are not applicable in MC simulations of double scattered PT¹⁴. Further, most MC studies of LET calculations for clinical double scattered PT have focused on brain and other tumour sites with shorter ranged treatment fields, and have therefore not implemented geometry used in calculations of longer ranged treatment fields, such as those used in PT of prostate cancer.

MC simulations are usually not calculated in clinical practices due to the computational load¹⁵, however, the potential effects from LET can be mitigated by careful consideration of the beam angles and the locations of distal edges¹⁶. In pencil beam scanning PT of prostate cancer, the high LET region has been shown to not only lie in the distal end of the treatment field, but also at the lateral penumbra of the spread out Bragg Peak (SOBP) for pencil beam scanning¹⁷. In clinical practise with this modality, adjustments of beam directions are being used to modulate the total dose distribution, yet with uncertain implications for the associated LET distributions.

The aim of this study was therefore to initially implement the necessary geometry for re-calculations of treatment plans for prostate cancer, with verification of dose calculations to measurements, and subsequently to analyse the field-angle dependence on high-dose LET in both the rectum and bladder in a large patient cohort.

2. Materials and Methods

Fjæra et al. published a FLUKA Monte Carlo implementation of a double scattered PT treatment nozzle¹⁴. Their work was focused on paediatric brain dose and LET calculations where the treatment field range is typically below 16 cm, while deeper seated targets, such as prostate, can require treatment fields with ranges of more than 30 cm. The double scattering treatment nozzle studied could not span such treatment field ranges using a single set of range specific components^{14,18,19}. Therefore, to re-calculate treatment plans for prostate cancer PT with the MC model developed by Fjæra et al., we implemented and validated the required long range specific geometry.

2.1 The double scattering treatment nozzle

The operation of the double scattering PT delivery system investigated (IBA Universal nozzle, University of Florida Health Proton Therapy Institute, Jacksonville, Florida, USA) was characterised by the three following characteristics: the delivered dose, the spatial profile of the proton beam, and the energy distribution of the beam^{14,18,20(p20)}. The delivered dose was dependent on the monitor units delivered along with the output factor of the treatment field. The spatial profile was described by the field radius and the lateral shape of the beam. The spatial profile was reached by use of three main components, i) the beam was broadened through the second scattering shield, ii) narrowed by the variable collimators and the snout, and iii) conformed to the target shape by the treatment field specific aperture. The energy modulation of the beam was performed primarily by two components, i) the rotation of the range modulation wheel which broadened the energy distribution to match the required SOBP, and ii) the treatment field specific range compensator which conformed the energy distribution to match the distal shape of the target.

Of the mentioned components, two long-range specific range modulation wheels needed implementation and following dose validation in this study. A more detailed description of the double scattering nozzle was published by Fjæra et al. in 2020 (see also Figure 1).

2.2 Implementation and validation of range modulation wheels

Two long-range specific range-modulation wheels were used under treatments of prostate cancer and required implementation into the FLUKA MC code. The range-modulation wheels were implemented according to manufacturer blueprints, and each consisted of three plates: An upstream plate made from a low-Z material (Lexan and Carbon), a centre plate made from aluminium and a downstream plate made of lead. The aluminium centre plates had fixed thicknesses of 1 mm, while the up- and down-stream plates had steps of increasing and decreasing thicknesses around the circumference of the plate, respectively. To ensure no overlap of the largest and smallest range pull-back, the upstream plate had a brass block between the thickest and thinnest step. All components were implemented in FLUKA using the Flair geoviewer²¹ as cylinders with each step of the up- and down-stream plates implemented as a single cylinder confined to the angular segment of the individual step. The zero-angle of the range modulation wheels was not supplied in the blueprints and had to be estimated through matching dose-depth simulations with dose-depth measurements.

The SOBP modulation width of each field delivery was translated into a rotation angle of the range

modulation wheel, starting at the zero-angle. To ensure a consistent energy modulation, the zero angle of the beam was within the angular segment of the brass block when the beam was turned on. After the beam was turned on, the range modulation wheels were rotated an angle equivalent to the rotation angle, defined from the requested modulation width. After this rotation, the beam was turned off and returned to the zero-angle. This was repeated several times per SOBP, and combined with beam current modulation resulted in a flat SOBP. The final position of the proton beam on the range modulation wheel, and thus also the modulation-width of the delivered SOBP, was therefore dependent on the requested SOBP as well as the zero-angle. Therefore, by comparing measured SOBPs with simulated SOBPs we could deduce whether our simulation employed a zero-angle too small or too large, and subsequently iterate our estimation of the zero-angle.

We defined the range as the range to the distal D80%, and we defined the modulation width as the range from the proximal D90% to the distal D90%. We aimed for range differences below 1 mm, and modulation width differences below 2 mm.

The measurements were obtained according to the procedure by Fjæra et al.¹⁴ and employed a square aperture with an opening of 15 cm x 15 cm and an air gap of 10 cm. The dose was measured with an IBA PPC05 parallel plate ionization chamber with 1 cm collection diameter, placed in an IBA Blue Phantom water phantom and irradiated with a gantry angle of 0 degrees to avoid the phantom wall. The depth wise measurements were conducted every 0.5 mm. Five measurements were conducted for one range modulator and six for the other, for 11 total SOBP irradiations over the two range modulators.

We performed FLUKA MC simulations with the same setup as the measurements, and scored dose in a cylinder with a diameter of 2 cm and a depth wise resolution of 0.5 mm, along the path of the proton beam. The dose was normalized to the mean dose in the centre of the SOBP +- 25% of the requested modulation width. We employed an iterative search through zero-angles, and started with an angle of 0 degrees, using 10 million primaries per simulation. As the differences in modulation-widths between the calculations and the measurements reached a minimum, we moved over to a grid search of +-3.5 degrees in the vicinity of the minimum, with 0.5 degree spacing, and 100 million primaries per simulation. All simulations were conducted with FLUKA2021.2.x, using the default HADROTHE settings.

2.4 Field angle dependence on LET

Dose and LET distributions were calculated for 582 prostate cancer patients using the FLUKA MC implementation, in order to study the relation between field configuration and dose and LET metrics. All patients were treated using the implemented double scattering PT nozzle at University of Florida Health Proton Therapy Institute (UFHPTI) in the years 2006-2010 in an IRB approved protocol (IRB201700516) with either lateral opposing fields, symmetric anterior oblique fields or symmetric posterior oblique fields.

The clinical target volumes (CTVs) included the prostate for both low, intermediate and high-risk patients, while also the proximal 2 cm of the seminal vesicles were included in the CTV for the intermediate and high-risk patients. The patients were planned using a planning target volume (PTV) with an 8 mm margin in the superior-inferior directions and a 6 mm margin in axial directions (lowered to 6 mm and 4 mm, respectively, post May 2008).

For each patient, the clinical treatment plan was recalculated using FLUKA MC with 200 million primaries per treatment field, scoring dose and dose averaged LET in water for all protons in the planning dose distribution grid, with FLUKA MC dose normalised to the median planning dose in the CTV.

We compared the mean LET in the 10 and 70 Gy isodoses of the bladder and rectum across all patients grouped by treatment field configurations into three groups: anterior oblique, lateral opposing and posterior oblique. Moreover, we calculated the mean LET, $\mu_{\text{LET}}(D_T)$, for all voxels of the bladder and rectum receiving more than a threshold dose, D_T , for D_T ranging from 0 to 80 Gy in steps of 0.1 Gy. We

compared the ratio of $\mu_{LET}(D_T)$ in the bladder and rectum between patients with anterior oblique, direct lateral opposing and posterior oblique field configurations. In total there were nine unique field angle configurations over all patients ($n=582$), with five different configurations in the anterior oblique group ($n=471$), one in the lateral opposing ($n=37$), and three in the posterior oblique group ($n=74$). We compared the groups using 95% confidence intervals, and we checked for normality at each dose level using qq-plots.

3. Results

3.1 Implementation and validation of range modulation wheels

The best fitting zero-angles were identified in the iterative search, resulting in SOBP ranges within 1 mm of measurements for all SOBPs, and nine of eleven simulated SOBP modulation widths within 2 mm of measurements, see Figure 2 for the zero-angle dependence of range modulation wheel 1. The two SOBPs with the largest differences in modulation widths had deviations of 7.7 mm and 24.0 mm, while all simulated SOBPs were visually close to measurements apart from the proximal dose of long range fields, as seen in Figure 3 for range-modulation wheels 1 and Supplementary Figure B for range-modulation wheel 2. The best fitting zero-angles were chosen as 16.0 deg and 28.0 deg for range-modulation wheels 1 and 2 respectively. A full overview of the ranges and modulation widths, as well as the differences between simulations and measurements can be found in table 1, and the validation data for range-modulation wheel 2 can be found in supplementary material (Supplementary Figures A and B respectively).

3.2 Field angle dependence on LET

The accuracy of the patient simulations (Figure 4) on a 3mm / 3% gamma pass requirement had a mean value of 95.4 % in the body with the 2mm / 2 % requirement yielding a mean value of 89 %. The PTV, bladder and rectum all had mean values of > 98 % for a 3mm / 3% requirement and values of > 93.8 % on a 2mm / 2% requirement. All simulations resulted in mean statistical uncertainties below 1% in the CTV.

The mean LET values in the bladder were generally larger than the mean LET values in the rectum for the patients treated with posterior oblique fields, as seen in Figure 5, with median-differences (calculated as rectum - bladder) in the 10 Gy isodose of -0.22 keV/um, 0.08 keV/um and 0.19 keV/um for the posterior oblique, lateral opposing and the anterior oblique groups respectively. In the 70 Gy isodose the same trend was seen, however the differences were less pronounced, with median-differences of -0.11 keV/um, 0.06 keV/um and 0.13 keV/um for the same three groups.

As shown in Figure 6, the ratio of $\mu_{LET}(D_T)$ between the bladder and rectum was largest in the posterior oblique group for all dose thresholds, with a maximum of 1.13 at a dose threshold of 9.6 Gy, while the anterior oblique group had the lowest ratio for all dose thresholds, with a minimum of 0.91 at a dose threshold of 5.2 Gy. The $\mu_{LET}(D_T)$ in the posterior oblique group was highest in the bladder for all dose thresholds, while it was highest in the rectum for all dose thresholds in the anterior oblique group. The lateral opposing group had ratios in-between the anterior oblique and posterior oblique groups for all dose thresholds, and showed higher $\mu_{LET}(D_T)$ in the rectum for all dose thresholds. The ratio of $\mu_{LET}(D_T)$ between the bladder and rectum was monotonously decreasing past the maximum for the posterior oblique group with the opposite effect observed in the anterior oblique group. The lateral opposing group displayed a flat profile of the ratio of $\mu_{LET}(D_T)$ between the bladder and rectum.

4. Discussion

In this study, we implemented and validated the long-range components in a double scattering PT nozzle using FLUKA MC. Good agreement with measurements was achieved. We subsequently used this implementation to calculate dose and LET in 582 prostate cancer patients with symmetric near-opposing field configurations and examined the differences in low- and high-dose LET and the mean LET ratio between the bladder and the rectum across field angle configurations. Furthermore we found clear differences in bladder and rectum LET across anterior oblique, lateral opposing and posterior oblique treatment fields.

The range and modulation width accuracy objectives of less than 1 mm and 2 mm differences, respectively, were met in all but two scenarios, where the MC calculated modulation-widths were too large – all MC calculated ranges were within 1 mm. The scenarios with too large MC calculated modulation-widths were for treatment fields with large requested modulation widths of over 15 cm, and while the modulation width differences were 7.7 mm and 24.0 mm, visual inspection of the SOBPs (Figure 3 and supplementary Figure B) revealed that the discrepancies were primarily in the proximal dose region. These results were similar to what has been found in other MC implementations of double scattering treatment nozzles, and the cause can likely be attributed to the definition of the modulation width^{14,18,22–24}. We defined the modulation width as the distance from the distal D90% to the proximal D90% which for fields with large modulation widths also included parts of the proximal build-up region. To mitigate this, we could have defined the modulation width as the distance from the proximal D98% to the distal D90%, limiting the defined area to the flat parts of the SOBP²⁵.

Differences in mean LET values of the rectum and bladder within the 10 Gy isodose varied between -0.22 keV/um and 0.19 keV/um across the three field angle configurations. These differences are generally small and would account for a difference of 0.01 in RBE when using the Unkelbach RBE model²⁶ with c=0.04. This difference is very small, and the clinical significance is likely minimal, with a potential dose difference below 1 Gy for the dose levels in the bladder and rectum. There was a systematic difference between the anterior oblique and posterior oblique treatment fields and while our study does not investigate individual field angles, we do expect this difference to be increasing with further treatment field angulation.

Furthermore, we calculated $\mu_{\text{LET}}(D_T)$, for the bladder and rectum of all 582 patients. We found no overlap of the 95% confidence intervals of the groups. This confirmed our hypothesis that the LET_D distributions of the rectum and bladder will be systematically different between especially anterior oblique and posterior oblique treatment configurations across a larger cohort of patients. A result similar to this was also shown by Pedersen et al in 2017¹⁷ for a single patient with pencil beam scanning PT. We expect these differences in bladder to rectum ratios of $\mu_{\text{LET}}(D_T)$ to generalise across individual field angles, however we were not able to show this using our dataset as some field angles had only been used in few cases.

The MC simulations used in this study were simulated with 200 million primaries per treatment field to ensure adequate statistical uncertainty. The simulation was conducted on a highly parallelised distributed computing system available in our institution, and took an estimated 1.5 hours per patient exclusively for the FLUKA MC simulation. The number of primary particles and the resulting simulation times were chosen based on achieving mean statistical uncertainties below 1% in the PTV^{19,20}.

In this study, we report the mean LET_D of volumes receiving more than D_T Gy as a function of the field configurations observed in this patient cohort. The field configurations in this cohort are not distributed evenly, as the patients were treated with a general focus on lowering the rectum dose, and thus employ mostly anterior oblique fields – furthermore, a large portion of this cohort were treated with the same field configuration of 85/275. Other studies into LET and field angles do exist^{17,27}, but these have primarily been planning studies on singular patient geometries, so while our cohort is skewed towards anterior oblique fields this analysis provides an overview of actual dose and LET distributions in larger patient cohorts treated with double scattered PT with symmetric near-opposing fields.

5. Conclusion

We implemented and validated the necessary FLUKA MC code to perform dose and LET calculations on a double scattered PT prostate cancer cohort. We achieved an overall good accuracy when comparing to measurements, thus allowing for dose and LET calculations in patients. We performed 582 patient treatment simulations and reported mean LET_D above a range of dose thresholds in bladder and rectum and we found a systematic difference in the mean LET values of the bladder and rectum as well as the bladder to rectum ratio of mean LET_D between anterior oblique, lateral opposing and posterior oblique treatment configurations.

Tables

Table 1: Overview of all measured and simulated SOBPs with their requested ranges and modulation widths along with the differences between measurements and FLUKA MC calculations, calculated as the FLUKA MC results subtracted from the measurements.

Modulation wheel	Requested range [cm]	Requested modulation width [cm]	Difference modulation width [cm]	Difference modulation width [cm]
1	19.84	3.00	0.03	0.67
	20.74	11.50	-0.47	0.91
	21.87	15.90	-0.04	7.72
	22.1	6.00	0.53	-0.93
	23.46	11.00	0.42	-0.16
	23.91	16.00	-0.21	-0.43
2	22.9	5.00	-0.33	0.43
	25.61	3.00	0.12	-0.89
	26.29	8.46	0.14	-0.23
	28.32	2.50	-0.34	-0.27
	28.4	15.90	-0.22	24.00

Figures

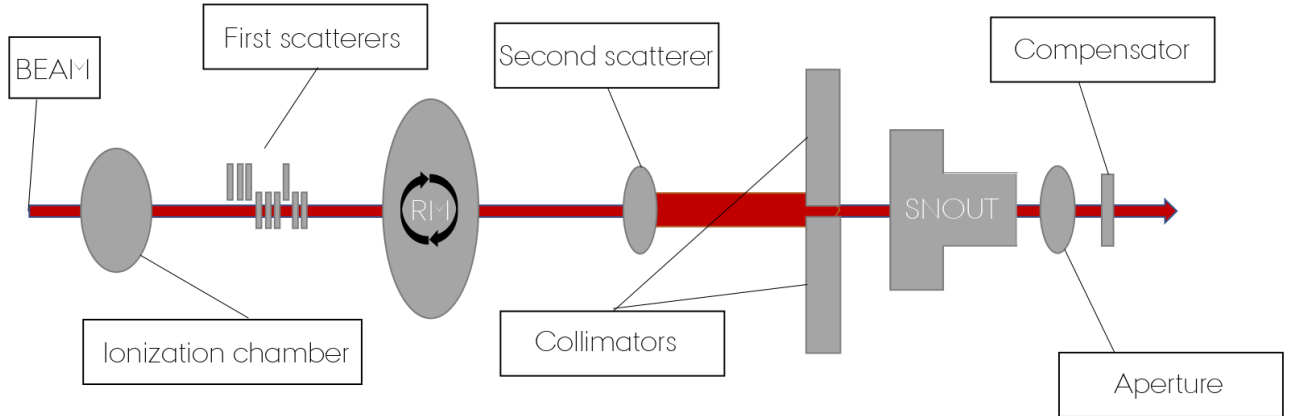


Figure 1: Sketch of the double scattering proton therapy treatment nozzle. Distances and sizes are not to scale, and not all components are shown. The proton beam is travelling left to right and shown as the red line.

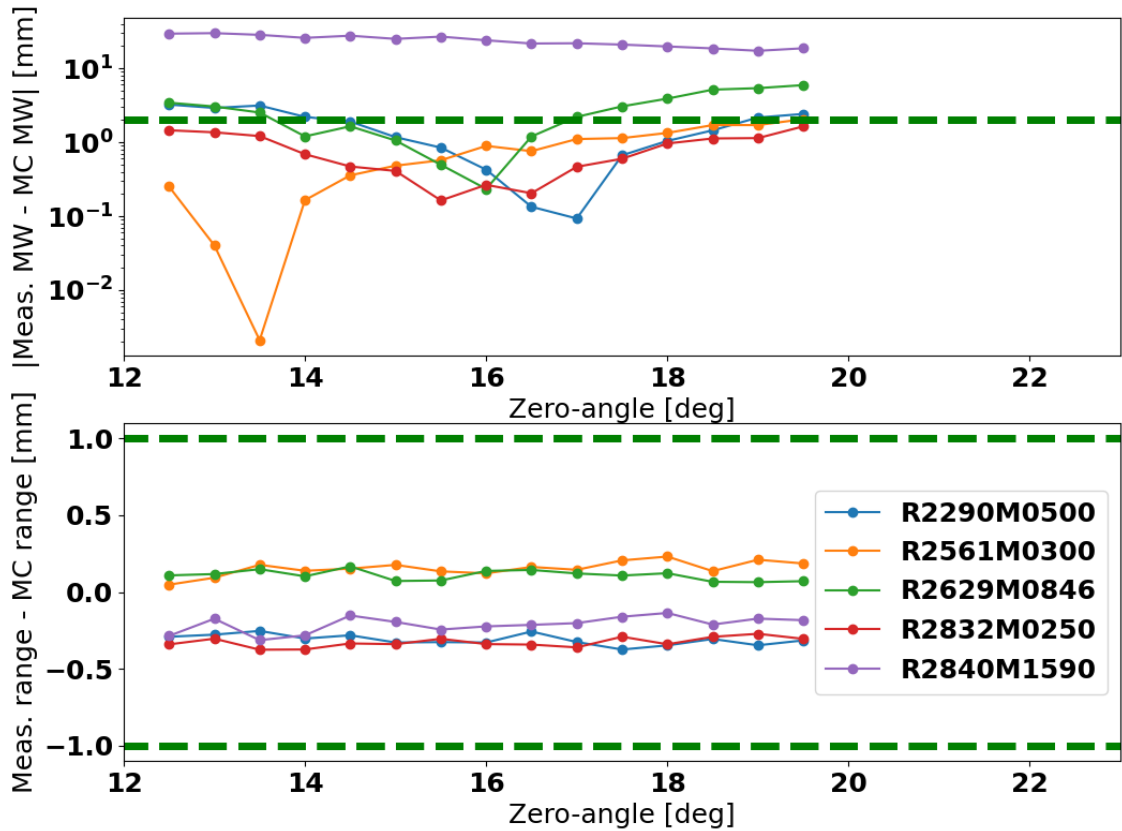


Figure 2: Top-panel: Absolute differences in modulation widths (MW) between FLUKA MC simulations and measurements as a function of MC simulation zero-angle for range-modulation wheel 1. Note the dashed green line indicating a difference of 2 mm. Bottom panel: Range differences between FLUKA MC simulations and measurements as a function of MC simulation zero-angle for range-modulation wheel 1. The difference is calculated as the FLUKA MC range subtracted from the measured range and the dashed green lines indicate plus and minus 1 mm range. The requested ranges and modulation widths are written as RxxxxMyyyy, where xxxx is the range in mm and yyyy is the modulation width in mm.

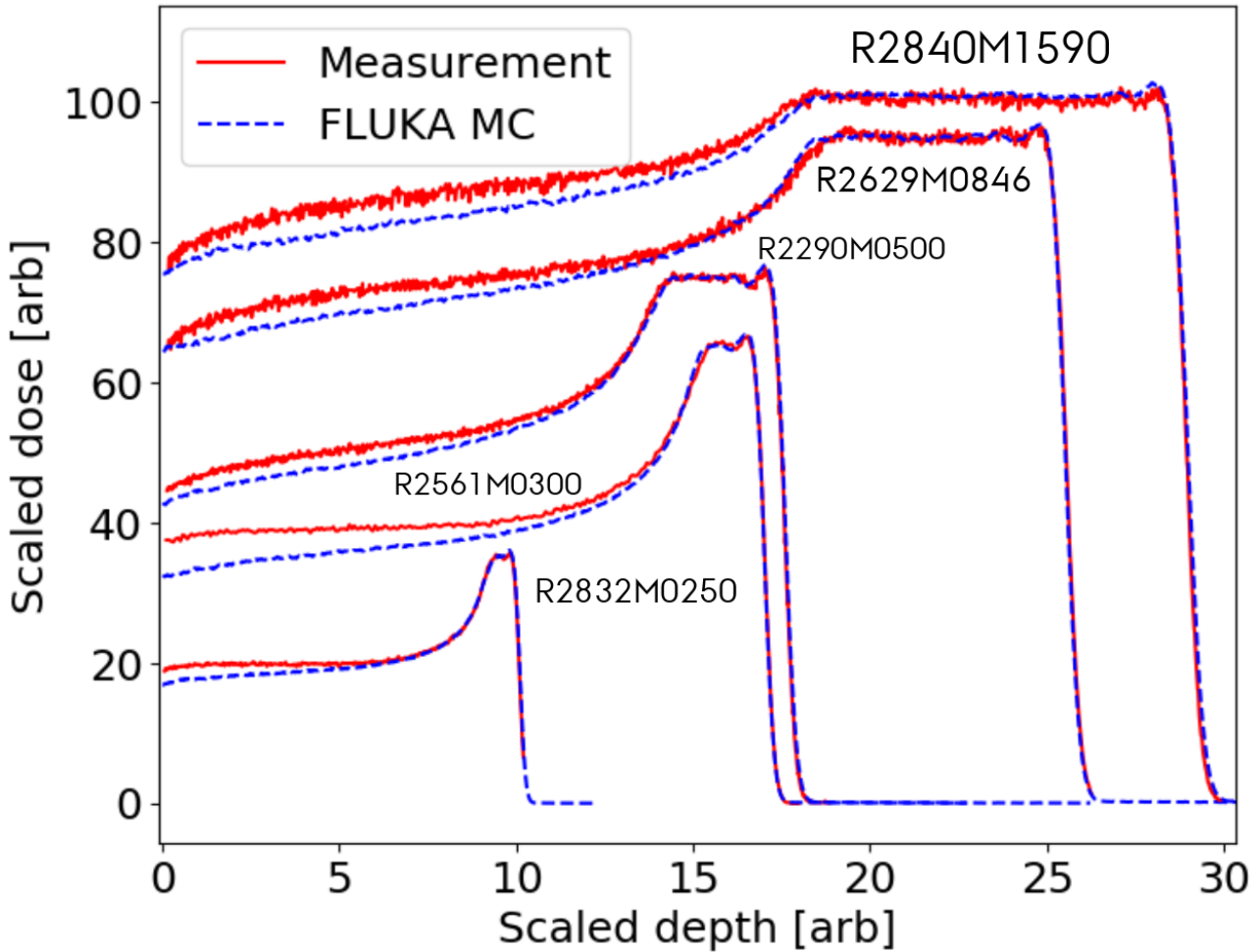


Figure 3: Dose depth curves for all measured and simulated SOBPs using range modulation wheel 1. The dashed blue lines represent the FLUKA MC calculated dose, and the red line represents measurements. Note that the doses and depths have been scaled such that all SOBPs fit in the figure. The requested ranges and modulation widths are written as RxxxxMyyyy, where xxxx is the range in mm and yyyy is the modulation width in mm.

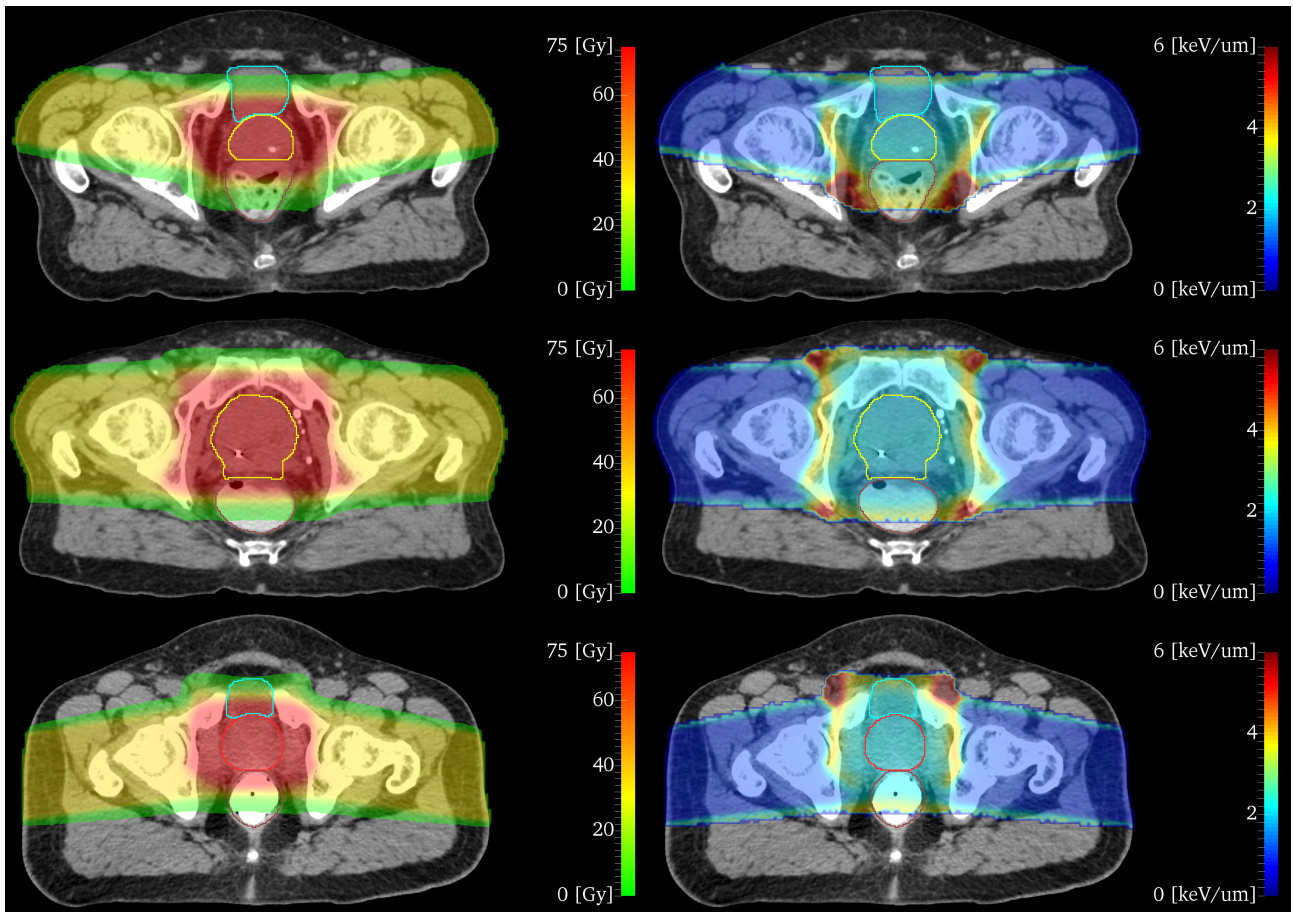


Figure 4: Dose and LET_D distributions for three patients, shown in the central axial plane of the prostate. Contours are, from the bottom to the top of each picture, rectum, CTV and bladder (if present). Only voxels receiving more than 2 Gy are shown. Top row: Patient treated with anterior oblique fields (82/278). Middle row: Patient treated with lateral opposing beams (90/270). Bottom row: Patient treated with posterior oblique fields (98/262).

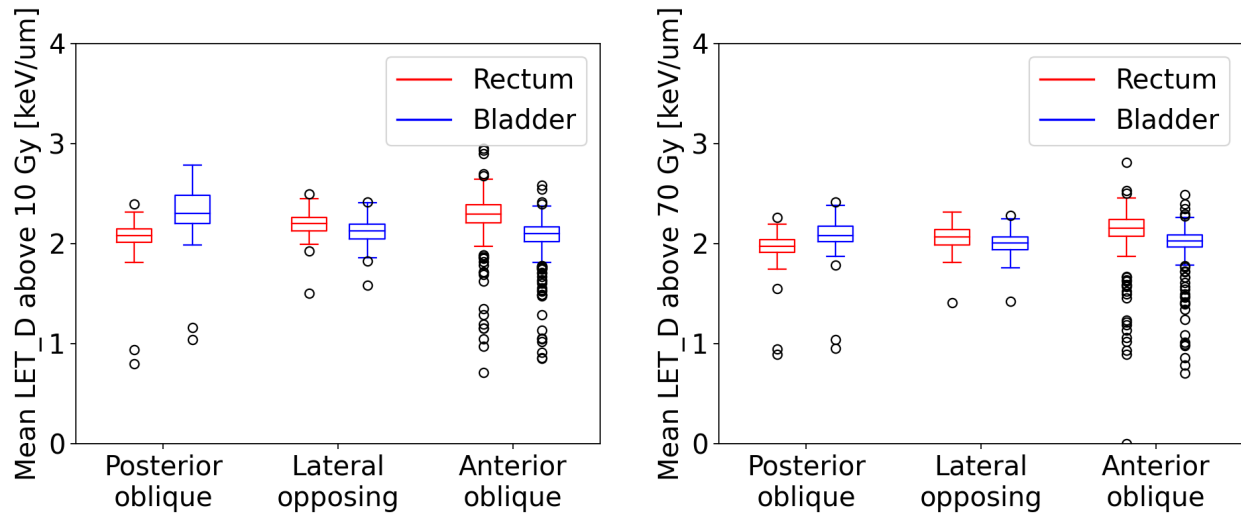


Figure 5: Boxplots of mean LET_D above two dose thresholds in the rectum (orange) and bladder (blue) for patients treated with symmetric anterior oblique, lateral opposing or symmetric posterior oblique fields. The dose thresholds used were 10 Gy and 70 Gy in the left and right panel, respectively. The posterior oblique group accounts for 26 patients, while the lateral opposing and anterior oblique groups contain 13 and 130 patients, respectively.

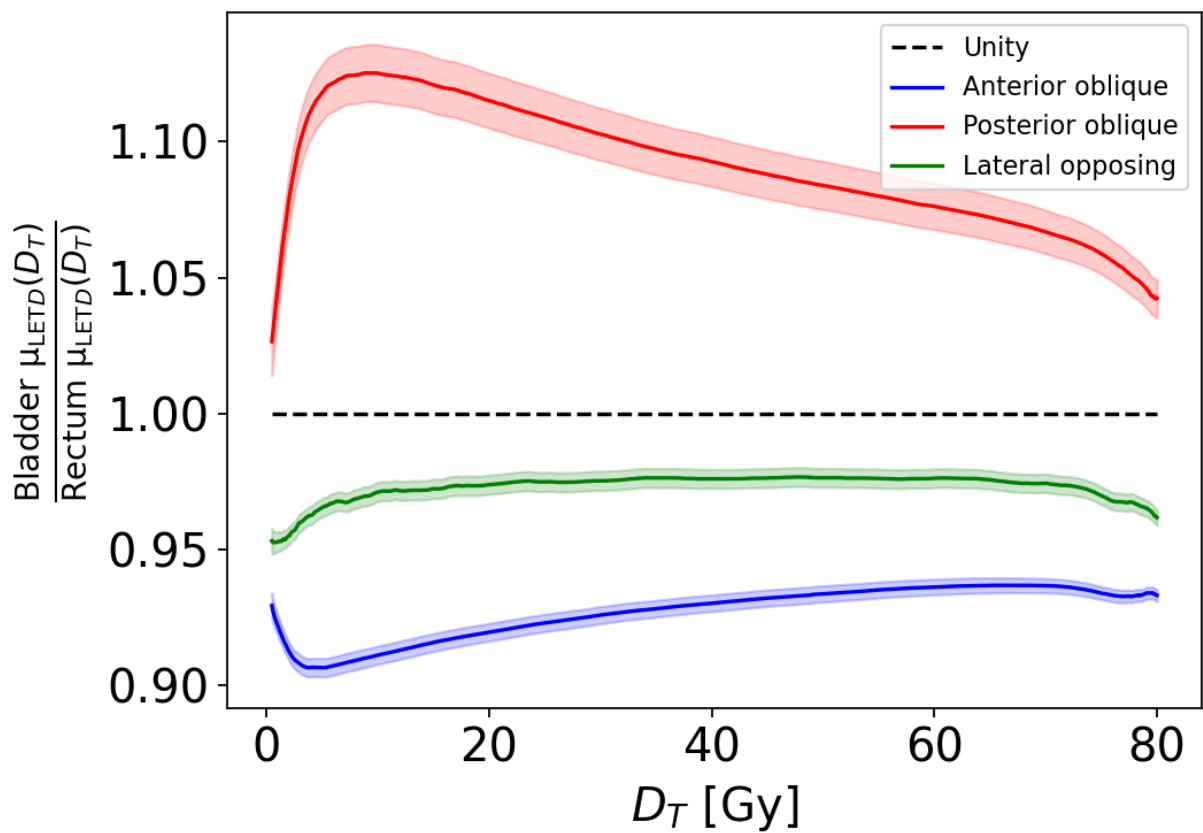


Figure 6: Ratio of $\mu_{\text{LETD}}(D_T)$ between bladder and rectum for all patients, grouped into anterior oblique, lateral opposing and posterior oblique fields scattering (blue, green and red, respectively). The shaded regions represent the 95% confidence interval in each patient group. The black, dashed line represents a ratio of 1, indicating an equal ratio.

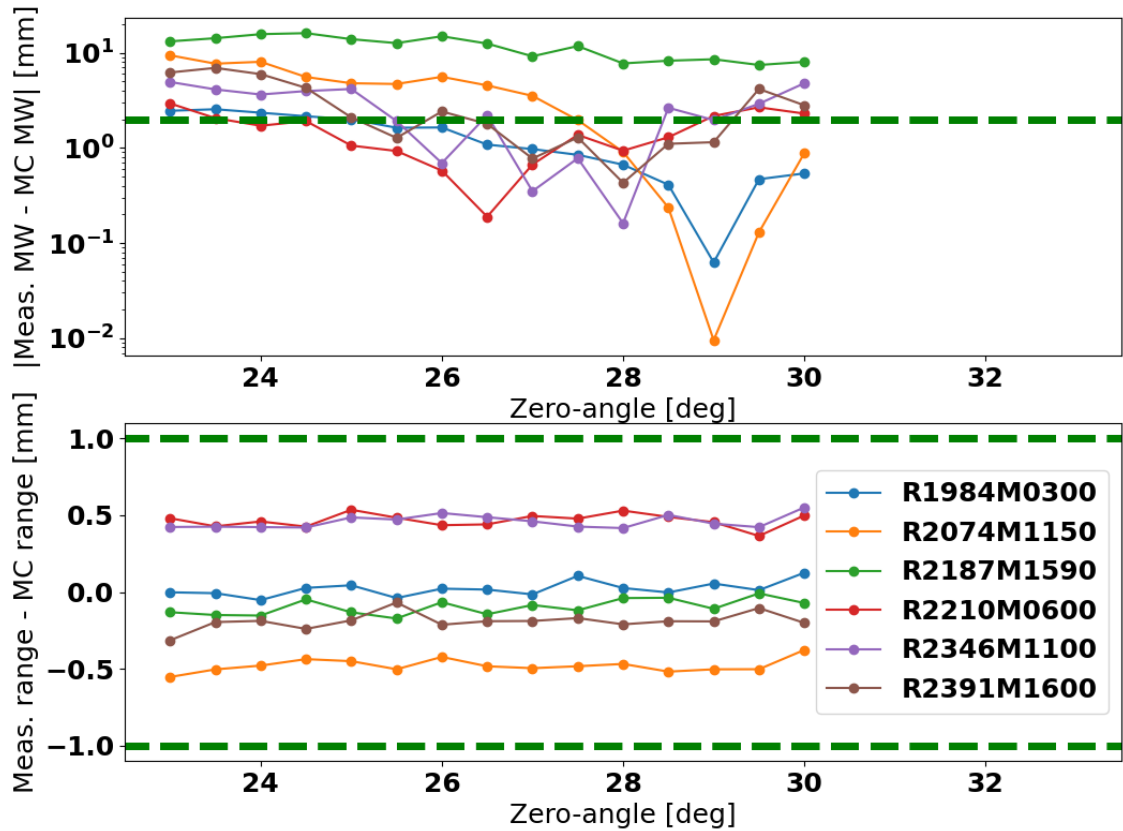
Bibliography

1. Protons vs. Photons for High-risk Prostate Cancer. Accessed April 4, 2024. <https://clinicaltrials.gov/study/NCT05350475>
2. Docetaxel, Androgen Deprivation and Proton Therapy for High Risk Prostate Cancer (PR05). Accessed April 4, 2024. <https://clinicaltrials.gov/study/NCT01040624>
3. Radiation Therapy (Hypofractionated Proton Beam Therapy or IMRT) for the Treatment of Recurrent, Oligometastatic Prostate Cancer Following Primary Localized Treatment. Accessed April 4, 2024. <https://clinicaltrials.gov/study/NCT04190446>
4. Dose-Escalated Proton Radiation Therapy for High-Risk Prostate Cancer (PR11). Accessed April 4, 2024. <https://clinicaltrials.gov/study/NCT03624660>
5. Proton Radiation Therapy for the Treatment of Patients With High Risk Prostate Cancer. Accessed April 4, 2024. <https://clinicaltrials.gov/study/NCT04725903>
6. Prospective Evaluation of Hypofractionation Proton Beam Therapy With Concurrent Treatment of the Prostate and Pelvic Nodes for Clinically Localized, High Risk or Unfavorable Intermediate Risk Prostate Cancer. Accessed April 4, 2024. <https://clinicaltrials.gov/study/NCT02874014>
7. ICRU 2007. Prescribing, Recording, and Reporting Proton-Beam Therapy. doi:10.1093/jicru_ndm021
8. Paganetti H. Relative biological effectiveness (RBE) values for proton beam therapy. Variations as a function of biological endpoint, dose, and linear energy transfer. *Phys Med Biol.* 2014;59(22):R419. doi:10.1088/0031-9155/59/22/R419
9. Liu C, Bradley JA, Zheng D, et al. RBE-weighted dose and its impact on the risk of acute coronary event for breast cancer patients treated with intensity modulated proton therapy. *J Appl Clin Med Phys.* 2022;23(4):e13527. doi:10.1002/acm2.13527
10. Mein S, Kopp B, Vela A, et al. How can we consider variable RBE and LETd prediction during clinical practice? A pediatric case report at the Normandy Proton Therapy Centre using an independent dose engine. *Radiat Oncol Lond Engl.* 2022;17(1):23. doi:10.1186/s13014-021-01960-w
11. Ödén J, Eriksson K, Toma-Dasu I. Inclusion of a variable RBE into proton and photon plan comparison for various fractionation schedules in prostate radiation therapy. *Med Phys.* 2017;44(3):810-822. doi:10.1002/mp.12117
12. Underwood TSA, McNamara AL, Appelt A, Haviland JS, Sørensen BS, Troost EGC. A systematic review of clinical studies on variable proton Relative Biological Effectiveness (RBE). *Radiother Oncol.* 2022;175:79-92. doi:10.1016/j.radonc.2022.08.014
13. Yang Y, Muller OM, Shiraishi S, et al. Empirical Relative Biological Effectiveness (RBE) for Mandible Osteoradionecrosis (ORN) in Head and Neck Cancer Patients Treated With Pencil-Beam-Scanning Proton Therapy (PBSPT): A Retrospective, Case-Matched Cohort Study. *Front Oncol.* 2022;12:843175. doi:10.3389/fonc.2022.843175

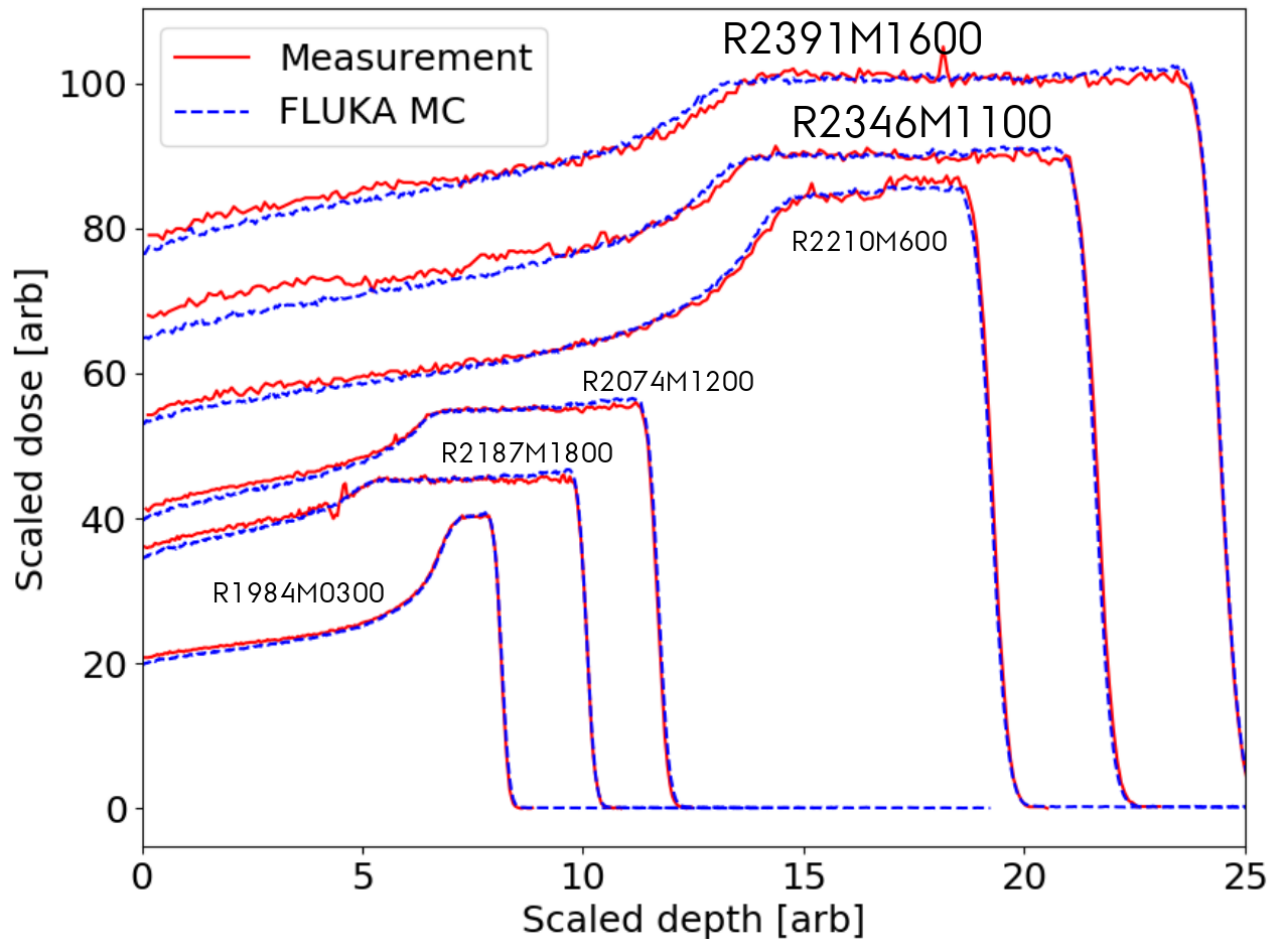
- 14.Fjæra LF, Indelicato DJ, Stokkevåg CH, Muren LP, Hsi WC, Ytre-Hauge KS. Implementation of a double scattering nozzle for Monte Carlo recalculation of proton plans with variable relative biological effectiveness. *Phys Med Biol.* 2020;65(22). doi:10.1088/1361-6560/abc12d
- 15.Kalholm F, Grzanka L, Traneus E, Bassler N. A systematic review on the usage of averaged LET in radiation biology for particle therapy. *Radiother Oncol.* 2021;161:211-221. doi:10.1016/j.radonc.2021.04.007
- 16.Haas-Kogan D, Indelicato D, Paganetti H, et al. National Cancer Institute Workshop on Proton Therapy for Children: Considerations Regarding Brainstem Injury. *Int J Radiat Oncol Biol Phys.* 2018;101(1):152-168. doi:10.1016/j.ijrobp.2018.01.013
- 17.Pedersen J, Petersen JBB, Stokkevåg CH, et al. Biological dose and complication probabilities for the rectum and bladder based on linear energy transfer distributions in spot scanning proton therapy of prostate cancer. *Acta Oncol.* 2017;56(11):1413-1419. doi:10.1080/0284186X.2017.1373198
- 18.Testa M, Schümann J, Lu HM, et al. Experimental validation of the TOPAS Monte Carlo system for passive scattering proton therapy. *Med Phys.* 2013;40(12):121719. doi:10.1118/1.4828781
- 19.Méndez JR, Perl J, Schuemann J, Shin J, Paganetti H, Faddegon B. Improved efficiency in Monte Carlo simulation for passive-scattering proton therapy. *Phys Med Biol.* 2015;60(13):5019-5035. doi:10.1088/0031-9155/60/13/5019
- 20.Bednarz B, Lu HM, Engelsman M, Paganetti H. Uncertainties and correction methods when modeling passive scattering proton therapy treatment heads with Monte Carlo. *Phys Med Biol.* 2011;56(9):2837-2854. doi:10.1088/0031-9155/56/9/013
- 21.Vlachoudis V. FLAIR: a powerful but user friendly graphical interface for FLUKA. In: *Proc. Int. Conf. on Mathematics, Computational Methods & Reactor Physics (M&C 2009), Saratoga Springs, New York.* Vol 176. ; 2009. Accessed December 4, 2023.
http://cern.ch/flair/doc/Flair_MC2009.pdf
- 22.Lutz B, Eulitz J, Haneke-Swanson R, Enghardt W, Lühr A. Precision modeling of the IBA Universal Nozzle double scattering mode at the University Proton Therapy Dresden for Monte Carlo simulation. *J Instrum.* 2021;16(03):T03007. doi:10.1088/1748-0221/16/03/T03007
- 23.Yuan J, Ellis R, Machtay M. Technical Note: An approach to building a Monte Carlo simulation model for a double scattering proton beam system. *Med Phys.* 2018;45(6):2660-2666. doi:10.1002/mp.12895
- 24.Liu H, Li Z, Slopsema R, Hong L, Pei X, Xu XG. TOPAS Monte Carlo simulation for double scattering proton therapy and dosimetric evaluation. *Phys Med.* 2019;62:53-62. doi:10.1016/j.ejmp.2019.05.001
- 25.Engelsman M, Lu HM, Herrup D, Bussiere M, Kooy HM. Commissioning a passive-scattering proton therapy nozzle for accurate SOBP delivery. *Med Phys.* 2009;36(6):2172-2180. doi:10.1118/1.3121489
- 26.Unkelbach J, Botas P, Giantsoudi D, Gorissen BL, Paganetti H. Reoptimization of Intensity Modulated Proton Therapy Plans Based on Linear Energy Transfer. *Int J Radiat Oncol Biol Phys.* 2016;96(5):1097-1106. doi:10.1016/j.ijrobp.2016.08.038

- 27.An Y, Shan J, Patel SH, et al. Robust intensity-modulated proton therapy to reduce high linear energy transfer in organs at risk. *Med Phys*. 2017;44(12):6138-6147. doi:10.1002/mp.12610

Supplementary material



Supplementary figure A: Top-panel: Absolute differences in modulation widths (MW) between FLUKA MC simulations and measurements as a function of MC simulation zero-angle for range-modulation wheel 2. Note the dashed green line indicating a difference of 2 mm. Bottom panel: Range differences between FLUKA MC simulations and measurements as a function of MC simulation zero-angle for range-modulation wheel 2. The difference is calculated as the FLUKA MC range subtracted from the measured range and the dashed green lines indicate plus and minus 1 mm range. The requested ranges and modulation widths are written as RxxxxMyyyy, where xxxx is the range in mm and yyyy is the modulation width in mm.



Supplementary figure B: Dose depth curves for all measured and simulated SOBPs using range modulation wheel 2. The dashed blue lines represent the FLUKA MC calculated dose, and the red line represents measurements. Note that the doses and depths have been scaled such that all SOBPs fit in the figure. The requested ranges and modulation widths are written as RxxxxMyyyy, where xxxx is the range in mm and yyyy is the modulation width in mm.